TOPICAL REVIEW • **OPEN ACCESS**

Design requirements for human UHF magnets from the perspective of MRI scientists

OPEN ACCESS
IOP Publishing
Superconductor Science and Technology
Supercond. Sci. Technol. **37** (2024) 113001 (17pp)
https://doi.org/10.1088/1361-6668/ad7d3f

Topical Review

Design requirements for human UHF magnets from the perspective of MRI scientists

Mark E Ladd[1,2,3,4,*], **Harald H Quick**[4,5], **Klaus Scheffler**[6,7] and **Oliver Speck**[8,9,10,11]

[1] Medical Physics in Radiology, German Cancer Research Center (DKFZ), Heidelberg, Germany
[2] Faculty of Medicine, Heidelberg University, Heidelberg, Germany
[3] Faculty of Physics and Astronomy, Heidelberg University, Heidelberg, Germany
[4] Erwin L. Hahn Institute for MRI, University of Duisburg-Essen, Essen, Germany
[5] High-Field and Hybrid MR Imaging, University Hospital Essen, Essen, Germany
[6] Magnetic Resonance Center, Max Planck Institute for Biological Cybernetics, Tübingen, Germany
[7] Department of Biomedical Magnetic Resonance, University of Tübingen, Tübingen, Germany
[8] Department of Biomedical Magnetic Resonance, Otto von Guericke University Magdeburg, Magdeburg, Germany
[9] German Center for Neurodegenerative Diseases (DZNE), Magdeburg, Germany
[10] Center for Behavioural Brain Sciences, Magdeburg, Germany
[11] Leibniz Institute for Neurobiology (LIN), Magdeburg, Germany

E-mail: mark.ladd@dkfz.de

Received 22 April 2024, revised 5 September 2024
Accepted for publication 18 September 2024
Published 30 September 2024

Abstract

The highest magnetic field strength for human-sized magnetic resonance imaging (MRI) currently lies at 11.7 tesla. Given the opportunities for enhanced sensitivity and improved data quality at higher static magnetic fields, several initiatives around the world are pursuing the implementation of further human MRI systems at or above 11.7 tesla. In general, members of the magnetic resonance (MR) research community are not experts on magnet technology. However, the magnet is the technological heart of any MR system, and the MRI community is challenging the magnet research and design community to fulfill the current engineering gap in implementing large-bore, highly homogeneous and stabile magnets at field strengths that go beyond the performance capability of niobium–titanium. In this article, we present an overview of magnet design for such systems from the perspective of MR scientists. The underlying motivation and need for higher magnetic fields are briefly introduced, and system design considerations for the magnet as well as for the MRI subsystems such as the gradients, the shimming arrangement, and the radiofrequency hardware are presented. Finally, important limitations to higher magnetic fields from physiological considerations are described, operating under the assumption that any engineering or economic barriers to realizing such systems will be overcome.

Keywords: MRI, ultra-high field, extremely high field, 14 tesla

* Author to whom any correspondence should be addressed.

1. Historical development of magnetic resonance imaging (MRI) and emergence of ultra-high fields

1.1. History of MRI

The principle of magnetic resonance (MR) was discovered in 1946 by physicists Felix Bloch and Edward Mills Purcell, who found that atomic nuclei in a strong static magnetic field tilt when they are excited by a high-frequency (or radiofrequency, RF) pulsed electromagnetic field [1, 2]. Once this high-frequency field is turned off, the atoms return to their original state, releasing the absorbed energy. This discovery laid the physical foundation for MRI, earning Bloch and Purcell the Nobel Prize in Physics in 1952.

In 1950, Erwin L. Hahn demonstrated that atomic nuclei generate a 'spin echo' when excited with two successive RF pulses [3]. However, MR was still slow and imprecise until 1966, when researchers from Zurich, Richard Ernst and Weston Anderson, significantly enhanced MR sensitivity. They improved the RF pulse excitation and used the recently proposed Fast Fourier Transform to analyze the acquired resonance signals [4], making the MR method a thousand times faster and much more sensitive. Ernst received the Nobel Prize in Chemistry in 1991 for this achievement.

By the early 1970s, MR became a critical analytical method for solids, liquids, and gases. In 1971, American physician Raymond Damadian demonstrated that MR could distinguish between tumors and healthy tissue [5]. Modern MRI was born in 1973 when chemist Paul C. Lauterbur and physicist Sir Peter Mansfield visualized fluid-filled objects using magnetic field gradients to create spatially resolved images [6, 7]. Both received the Nobel Prize in Physiology or Medicine in 2003 for their pioneering work in MRI technology.

Commercial and clinically usable MRI systems for humans were introduced in the early 1980s. The first human-size superconducting magnets operated at 0.35 tesla (T) and 0.5 T, followed by 1.5 T systems. In 1987, Siemens installed the first 4 T whole-body MRI system for research on new diagnostic and imaging possibilities [8, 9]. Despite these rapid advancements, it was not until the early 2000s that 3 T MRI systems were broadly used clinically [10]. Today, most of the estimated 45 000 clinical MRI systems worldwide operate at 1.5 T or lower, with 3 T systems making up about 15%–18% of the installed base in Europe and North America [11, 12].

1.2. Emergence of ultra-high fields (UHFs)

MRI has seen a steady increase in magnetic field strength since its inception, as described above. Higher magnetic fields provide higher tissue magnetization, leading to better signal-to-noise ratio (SNR), enhanced MR image quality, increased spatial resolution, faster imaging, and greater sensitivity. Moreover, many tissue contrasts and the spectral separation between different chemical species also improve with higher magnetic fields, enhancing specificity. However, achieving higher fields requires technological feasibility, and superconducting magnet technology is the decisive precondition and key to achieve higher field strength.

The development of stronger superconducting magnets for human MRI led to the installation of an 8 T system in the late 1990s [13], followed by several 7 T MRI systems in 1999 and the 2000s. Human MRI systems operating at or above 7 T are generally referred to as UHFs. The largest UHF segment is at 7 T (300 MHz proton resonance frequency), with over 100 7 T systems installed worldwide since the first 7 T system received clinical CE and FDA approval in 2017 for brain and small joint examinations. Currently, two commercial vendors produce systems labeled for clinical use. There are also a few human research MRI systems operating at 9.4 T (400 MHz) [14].

The development of MRI magnets for human use has not stopped there. The next highest magnetic field MRI system currently in operation and generating images *in vivo* is located at the University of Minnesota. The system operates at 10.5 T (450 MHz proton resonance frequency) and was installed in 2013. However, it did not receive approval for *in vivo* imaging until 2017. The passively shielded 10.5 T magnet, one of the last produced by Agilent Technologies before the company exited the magnet market completely, uses 433 km of niobium–titanium (NbTi) wire cooled to below 3 K, weighs 110 tons, and has a 88 cm warm bore, making it suitable for human whole-body MR imaging. This 10.5 T MRI system is approved only for research use, with initial *in vivo* results in the human brain [15] and human torso [16].

The highest field whole-body MRI system is at NeuroSpin CEA Paris-Saclay, operating at 11.7 T (500 MHz proton resonance frequency) [17]. Developed by CEA and produced together with Alstom (now General Electric), the conceptualization of this system, known as the Iseult project, began in 2004 as a French-German cooperation. The magnet reached its target field in July 2019 and produced first images of test objects in 2021. The 11.7 T magnet uses an actively shielded double-pancake design in driven mode at 1470 A using NbTi wire cooled to 1.8 K with superfluid helium. With a warm bore of 90 cm, it is currently the largest 11.7 T human UHF MRI magnet worldwide, weighing 132 tons and measuring 5.2 m in length and 5 m in diameter [18]. A press release with the world's first 3D MR images of a human brain *in vivo* at 11.7 T was published in early April 2024 [19].

Two 11.7 T head-only MRI systems are currently being put into operation at the National Institutes of Health (NIH) in the USA and at Gachon Medical University in South Korea. The NIH magnet, initially produced by Agilent, was damaged during a quench event and later repaired by ASG Superconductors. In 2019, it was reinstalled at the NIH. The Gachon magnet was completely designed and manufactured by ASG. Although there are minor differences between the two magnets, both use approximately 600 km of NbTi wire, weigh 66 tons, utilize passive shielding, and provide a 70 cm warm bore [20]. The NIH system is shielded with 380 tons of iron. The Gachon system has reached field but is not yet producing *in vivo* images at the time of this writing, while the NIH system is in the process of being ramped.

In the UK, funding for an 11.7 T magnet has been announced [21]. This system will use NbTi wire cooled to 2.2 K [22] and will have an 83 cm warm bore capable of accommodating a whole-body gradient set. It will be passively shielded with approximately 500 tons of iron.

1.3. The future starts now: extremely high field (EHF) MRI initiatives

The superconducting technology for the construction of magnets with a magnetic field strength above 12 T must fundamentally change, as the superconducting properties of NbTi do not support such high magnetic fields. Hence, a new classification for human MRI systems with a magnetic field strength above 12 T is needed. Magnetic fields at or above 12 T are thus referred to as EHFs in the rest of this article to differentiate them from systems using NbTi technology.

In the Netherlands, a national initiative to establish a 14 T whole-body MRI system has recently received funding [23]. The world's strongest MRI system will be sited in Nijmegen and is based on a variant of a whole-body magnet design published by Li and Roell [24]. The magnet is currently being built by Neoscan Solutions in Magdeburg, Germany. This is the only current human UHF or EHF magnet design based on a high-temperature superconductor (HTS). As no similar magnet has ever been built before, it has to be demonstrated that the technology will function as planned.

Two further EHF projects have been announced in China during recent years. The Institute of Plasma Physics of the Chinese Academy of Sciences has declared its intention to design and construct a 14 T MRI magnet with 90 cm warm bore based on niobium-tin (Nb_3Sn) superconducting cables [25]. An additional group from the Chinese Academy of Sciences has published the basic design of a whole-body, actively shielded 14 T magnet [26].

Finally, the German Ultrahigh Field Imaging network has announced plans to pursue a 14 T whole-body MRI system as part of a national research facility [20].

2. Motivation for going to higher field strengths in MRI

The primary limitation of MRI is its low sensitivity, which stems from the low thermal equilibrium magnetization of tissues as dictated by the Boltzmann distribution. Increasing the static magnetic field strength is one way to address this limitation. In human MRI, the noise from the sample typically dominates over the electronic noise of the signal receiver. As a result, if wavelength effects are ignored and the quasi-static approximation is applied, the SNR is expected to increase linearly with magnetic field strength. However, considering the full Maxwell equations, theoretical and experimental work has demonstrated a supralinear increase in the UHF and EHF regimes. For instance, an *in vivo* brain MRI comparison at 3, 7, and 9.4 T revealed that SNR increases with magnetic field strength as $B_0^{1.65}$ in the cerebrum [27]. Another recent study measuring SNR in the center of a spherical phantom at 3, 7, 9.4, 10.5, and 11.7 T found that SNR grows as $B_0^{1.94\pm0.16}$ [28]. Furthermore, simulation studies on the ultimate intrinsic SNR in brain models suggest that SNR enhancement with increased magnetic field strength is spatially dependent, with faster increases for deeper tissues compared to peripheral tissues [29, 30].

A higher magnetic field strength also offers the benefit of greater separation between individual spectral peaks, allowing for the differentiation of a larger number of molecular species. This is crucial for studies that rely on the acquisition of metabolic or chemical spectroscopic profiles, both with hydrogen [31] and other nuclei [32, 33].

Scientists and clinicians aiming to use higher magnetic fields seek to improve the sensitivity or specificity of the MR imaging information to better address their research or diagnostic questions. When new field strengths are introduced, diagnostic applications can only be a long-term goal, as technical challenges need to be overcome and also the demonstration of diagnostic benefits in comparison to existing systems requires extensive investigation to justify the higher costs. Thus, for EHF systems, the primary goal is to answer fundamental questions about healthy physiology or ageing, but also to investigate pathologies in research cohorts. The systems are targeted toward pursuing questions in groups of subjects rather than providing diagnostically useful information in individuals. Whereas in North America new, higher fields strengths have traditionally been driven by cognitive neuroimaging questions and a focus on the brain [34–36], in Europe the interest has included early application to other parts of the body, heightening the interest in whole-body EHF systems [20, 23].

To illustrate the goals of going to higher magnetic field strength, in the following we present three selected examples where higher static magnetic fields have demonstrated quantifiable superiority over lower field strengths. For more extensive information on the full breadth of possible UHF applications, we refer to dedicated review articles addressing the specific advantages (and disadvantages) of UHF MR [37–43].

2.1. High-resolution structural imaging

The success of (clinical) MRI is based on its high information content in structural images. Superior native image contrast compared to other imaging modalities and a broad range of contrast-generating mechanisms can be exploited. For most applications, a compromise between spatial resolution, image contrast, and SNR has to be achieved. Improving spatial resolution in MRI is 'expensive' in terms of scan time. If more than sufficient SNR is available, the required number of encoding steps increases quadratically with the resolution improvement in 3D acquisitions, e.g. changing the voxel edge length from 1 mm to 0.5 mm requires 4-times longer scan time. If SNR is still high enough, undersampling methods may reduce this required scan time. If an acquisition is SNR-limited, however, the reduction in voxel volume requires an increase in scan time to compensate, where SNR is proportional to the square root of scan time, e.g. changing the voxel edge length from 1 mm

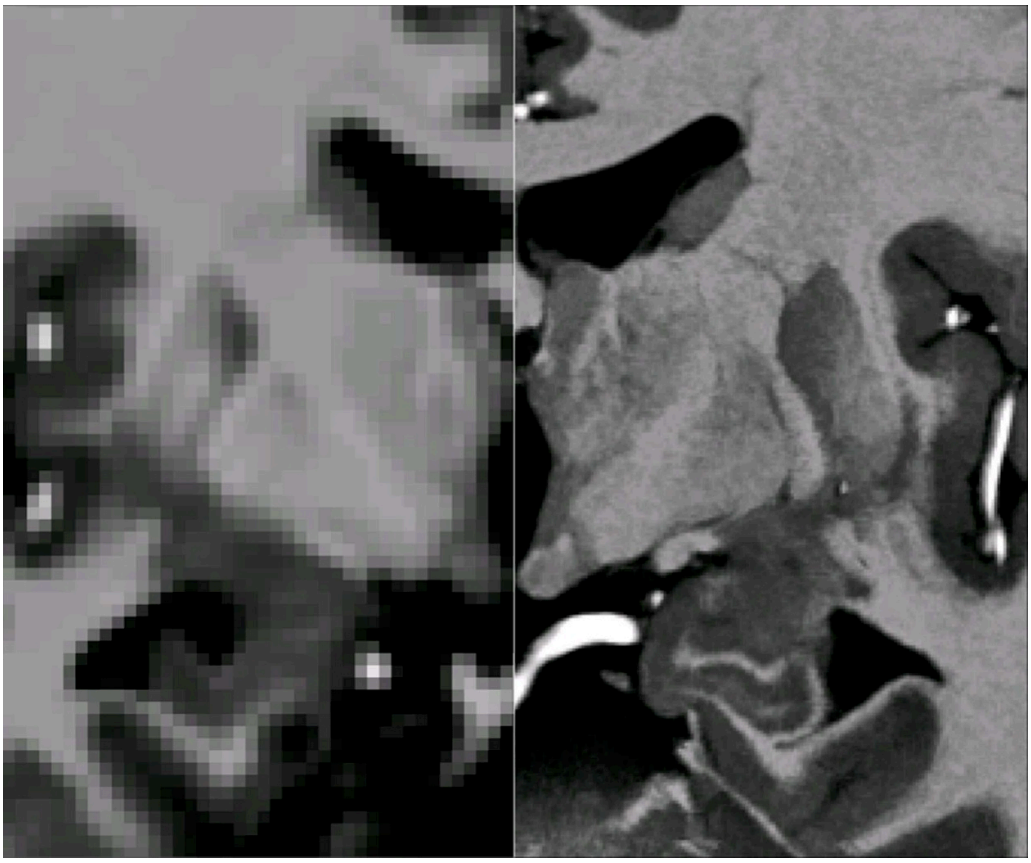

Figure 1. T1-weighted 1 mm isotropic resolution MRI at 7 T of the deep gray matter and medial temporal lobe region including hippocampus (left) compared to a very high resolution *in vivo* acquisition with 250 μm isotropic resolution (right). This high resolution measurement was enabled through the use of prospective motion correction during an extended scan time at 7 T as described by Lüsebrink *et al* [47].

to 0.5 mm and thus reducing the voxel volume by a factor 8 requires 64-times longer scan time.

As noted above, SNR increases with field strength. Assuming that the SNR is proportional to $B_0^{1.65}$ [27], doubling the field strength from 7 T to 14 T would result in an SNR increase by a factor 3.14, allowing a scan time reduction by a factor of about 10 compared to 7 T and about 160 compared to 3 T. Further factors, such as field strength dependent changes in relaxation times can compromise this gain, e.g. due to reduced $T2^*$, or even further contribute to higher SNR, e.g. longer T1 in time-of-flight angiography. Obviously, factors such as RF coil sensitivity or gradient performance will affect the sensitivity further.

With high spatial resolution and long scan times, subject motion becomes more relevant, and a number of approaches have been proposed to address motion related effective resolution loss, for example fat navigators [44], moiré phase tracking [45], or field probes [46]. An example of unprecedented high spatial resolution structural *in vivo* brain imaging has been presented with 250 μm resolution T1-weighted imaging at 7 T [47] (figure 1). While this acquisition took about 7 h, it could be expected to be feasible at 14 T within 45 min. Improvement through model-based or deep neural network-based denoising [48–50] may further reduce this time.

2.2. Functional MRI

A relevant driving force for moving to higher magnetic fields has been functional MRI. This is motivated by the increase in susceptibility effects that are the basis of the blood oxygen level dependent (BOLD) effect, which is the most frequently exploited contrast mechanism for detecting neuronal activation. This susceptibility sensitivity increase adds to the SNR increase. The gain in BOLD sensitivity varies between spin-echo based methods and gradient-echo (GE) based methods. In GE BOLD, the signal change is dominated by the static dephasing effects around vessels and leads to a linear or slightly supralinear increase in $\Delta R2^*$ with field strength, which has been demonstrated in humans up to 7 T and in rats up to 15.2 T [51, 52]. However, the relative change in relaxation rate only slightly increases with field strength due to reduced $T2^*$ at higher field. Correspondingly, the relative BOLD-related signal change increases mildly with field strength at TE equal to $T2^*$ or T2. Experimental results at high and very high fields have shown similar contrast-to-noise ratio once the measurement is limited by physiologic noise, diminishing the additional gain at higher field for moderate resolution. Thus, the gain can be fully exploited only if the BOLD measurement is in the regime dominated by thermal noise. This is relevant for highest spatial resolution functional MRI (figure 2). Such high

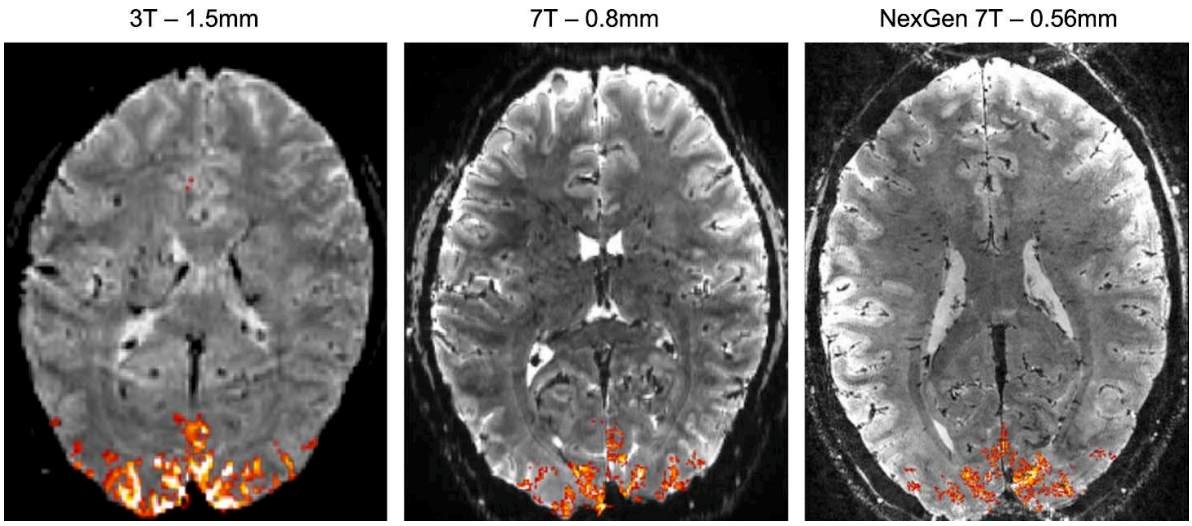

Figure 2. BOLD EPI acquisition of visual cortex activation with increasing spatial resolution (left to right) afforded by an increase in sensitivity through higher magnetic field strength ('standard' 7 T MRI, middle) and higher gradient performance together with high RF receiver channel count (NexGen 7 T, right). Images courtesy of D. Feinberg, A. Vu, A. Beckett, S. Park and S. Hakkinen, University of California Berkeley [55].

resolution (sub-millimeter) fMRI allows localization of neuronal activation not only along the cortical surface, such as in columnar mapping, but also in depth, such as in laminar fMRI [53]. Depth-dependent or laminar fMRI has gained significant interest, as different cortical layers process incoming and outgoing neuronal signals and thus add a directionality dimension to the cortical signal [54].

*2.3. Chemical exchange saturation transfer **(CEST)***

CEST is a relatively new MR imaging approach that enables the acquisition of information about small metabolites and proteins by looking at spectral information encoded onto the protons (^{1}H) of these molecules [56]. Substances detectable by CEST that have been reported include peptides and proteins, glycosaminoglycans in cartilage, creatine, glutamate, iopamidol, and glucose. However, in contrast to direct spectral imaging, CEST relies on transferring the information to the much larger water pool by the continuous exchange of protons between these molecules and water. By doing so, the available signal amplitude is enhanced by factors up to $>$1000 versus direct spectroscopy, and spectral images at the spatial resolution of conventional MR water images are achievable.

Nevertheless, despite the signal amplification, the technique is still signal starved due to the much lower concentration of protons outside the water pool. CEST effects are in general only in the range of a few percent of the water signal. Thus, UHF MR provides two significant benefits: 1) the strength of the signals is directly boosted, and 2) the separation between the peaks of individual resonances in the spectrum increases linearly with magnetic field strength, reducing spectral overlap and increasing selectivity. Figure 3 shows a comparison between a CEST Z-spectrum acquired at 3 T in the human brain and one acquired at 9.4 T in the mouse brain, showing the improvement in spectral quality. Nevertheless, inhomogeneities in the main magnetic field B_0 can lead to severe inaccuracies in the determination of CEST effects [57]. Given the generally stronger non-uniformities at high B_0, it is important to correct for these effects to profit from the other advantages (cf section 3.2).

3. Design considerations for human MRI systems $>$12 T

MR systems above 12 T represent a significant engineering challenge. To fulfill expectations for applying these systems for particular research questions, the magnet and other system components need to meet certain performance specifications. In the following, we discuss some general considerations for setting these specifications from the MR physics and application point of view. An overview of these design considerations, as discussed in the following subsections, is provided in table 1.

3.1. Magnet

The heart of any MR system is the magnet, and for MRI systems exceeding 12 T, the greatest technological hurdle is the magnet, as the other system components should be achievable by extending currently applied engineering solutions. A clear responsibility for the MR community is to answer what specifications should be considered when designing and building the magnet. This is not a completely straightforward question to answer. On the one hand, there are specifications that will be fairly absolute, such as the field strength to be achieved. On the other hand, there are many specifications for which there is no unambiguous target. For these parameters, there will be compromises that the community is willing to accommodate

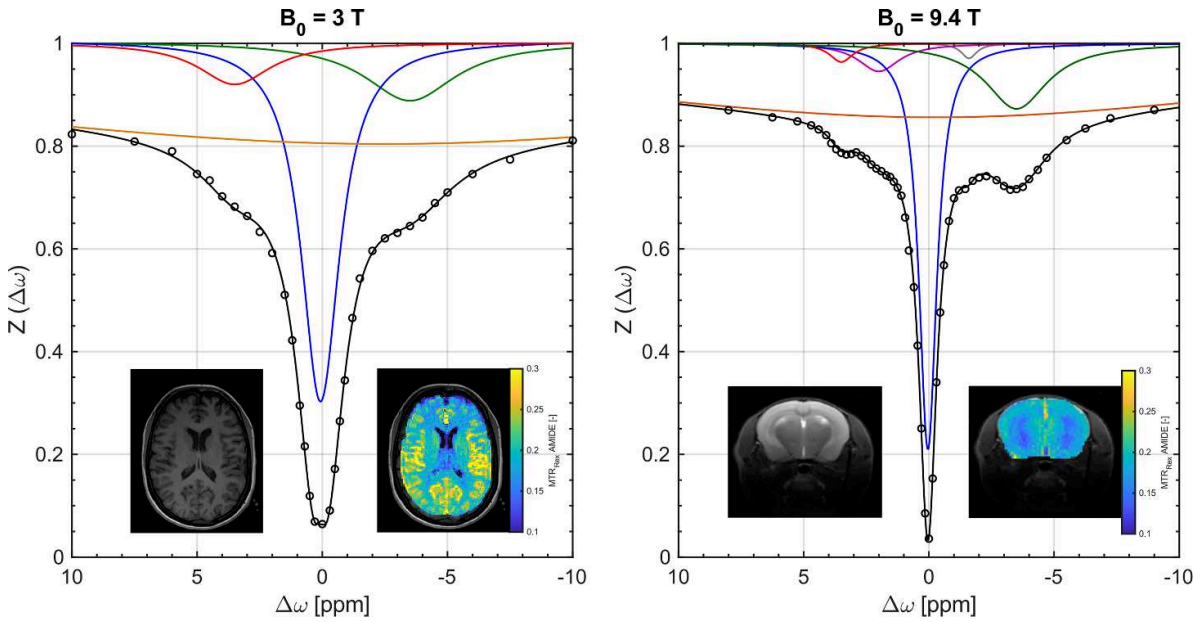

Figure 3. In CEST MRI, each image voxel corresponds to an individual Z-spectrum (black data points). The CEST signal of each fitted pool within the Z-spectrum (i.e. colored solid lines corresponding to different molecular entities of cellular components) can be visualized as an individual MR image. Most notably, the spectral resolution increases with increasing B_0 allowing not only for (i) enhanced sensitivity towards CEST signals but, more importantly, (ii) enhanced spectral specificity enabling separation of superimposing CEST signals. 3 T: brain of healthy volunteer; 9.4 T: brain of healthy mouse. Both Z-spectra are single-voxel Z-spectra, and both were acquired with a local saturation amplitude of $B_1 = 0.7$ μT. Insets represent high-resolution anatomical image (left) and isolated amide CEST image (right, MTR_{Rex} amide, i.e. corresponding to the red fitted line). Resolution of CEST images: 3 T = [1.70 x 1.70 × 3.0] mm^3, 9.4 T = [0.25 x 0.25 × 1.5] mm^3. Multi-pool Lorentzian fitting: blue = direct water saturation (DS; $\Delta\omega = 0$ ppm); orange = semi-solid magnetization transfer (ssMT; $\Delta\omega \approx -3$ ppm; i.e. semi-solid structures *in vivo*; e.g. cell membranes, surface proteins or the cytoskeleton); red = amide protons ($\Delta\omega \approx 3.5$ ppm; i.e. —NH; e.g. from the backbone of amino acid chains in mobile peptides and proteins); green = exchange-relayed nuclear Overhauser effect (rNOE; $\Delta\omega \approx -3.5$ ppm; i.e. non-exchanging, covalently bound aliphatic protons; e.g. from macromolecules); magenta = guanidino protons (only possible at UHF; $\Delta\omega \approx -2$ ppm; i.e. —$(NH_2)_2$+; e.g. from protein arginine or metabolites such as creatine); gray = second rNOE (only possible at UHF). Other acronyms: Z = normalized water signal, $\Delta\omega$ = frequency offset with respect to water signal, MTR_{Rex} = magnetization transfer ratio of exchange-dependent relaxation rate. Figure courtesy of P. Boyd, German Cancer Research Center, Heidelberg.

in the early phases of technology exploration. An example would be cryogen usage. Ideally the usage would be very low, going down to zero boil-off or even cryogenless, but for the first generation of these systems, elevated maintenance costs could be acceptable. Finally, there are specifications for which the community will have no clear preference as long as other specifications are met. For instance, a question from a magnet designer might be whether a driven design with the necessity to incorporate a power supply to compensate for residual resistive losses in the joints of the superconductors is acceptable. For the MR community, the most likely answer is that this is irrelevant, as long as the specifications for field stability can be met.

3.1.1. What field strength should be next? As mentioned in sections 1.2 and 1.3, there are several projects pursuing human MRI at field strengths at or above 10.5 T, either already in operation or nearing active imaging capability. The highest operational field strength is 11.7 T. At NeuroSpin and Gachon the magnets are at field, and NeuroSpin is performing initial human imaging; NIH is in the process of energizing the magnet. All of these magnets are based on NbTi superconductor, which is the most common low temperature superconductor used for human MRI magnets. Field strengths above 11.7 T are no longer realistically achievable with NbTi due to limitations in its critical field strength at liquid helium temperatures. A significant breakthrough would thus be the establishment of a human MRI system above 12 T based on a new superconductor technology like Nb_3Sn or HTS [60].

The 14 T magnet planned for Nijmegen is based on HTS. On the one hand, this target field strength is double 7 T, which is currently the largest cluster of active systems operating at UHF, so a significant sensitivity boost is expected. Also, it is comfortably in the zone requiring a new superconductor technology without overtaxing the upper limits of those superconductors. Successful demonstration will open a path to even higher magnetic fields after sufficient experience is gathered in this conservative operational range of the superconductor. Finally, beyond technological considerations, the ultimate upper limit on acceptable field strength will be set by physiological factors (cf. section 4.1). The jump in field strength between 11.7 T and 14 T is significant without being

Table 1. Overview of design considerations from an MRI perspective.

Parameter	Specification	Comment
Field strength	10.5 T whole-body and 11.7 whole-body already operational, 11.7 T head-only nearing operation, 14 T whole-body planned	Ultimate upper field strength will be determined by physiological constraints; stepwise increase preferable to evaluate safety concerns.
Superconductor material	NbTi up to 11.7 T, Nb_3Sn or HTS for >12 T	Great interest in making the transition to a new superconductor technology that might later be translated to lower field strengths or open path to even higher field strengths
Head-only vs. whole body	Head-only if research driven by cognitive neuroimaging; whole-body if medical research is a focus	A head-only system is also of interest for medical research, but it does restrict the research questions that can be pursued
Warm bore	$\geqslant$68 cm for head-only, $\geqslant$83 cm for whole-body	See text for more specific criteria
Homogeneity of shimmed magnet (empty)	$\leqslant$0.5 ppm peak-to-peak over 22–30 cm sphere	Ultimately, the homogeneity in the object under examination using additional resistive shims is determinant
Superconducting shims vs. passive shims	Either or both, as long as the homogeneity requirements are fulfilled	
Field stability (drift)	$\leqslant 0.05$ ppm h^{-1}	Additional field monitoring solutions may relax this requirement
Driven vs. persistent mode	Either as long as magnetic field stability criteria are fulfilled	A high-stability power supply or other measures will be necessary in the case of a driven design
Active or passive shielding	Either	Passive shield will generally be easier to implement, simplify quench management, and reduce the cost and size of the magnet; active shielding will simplify siting
Helium usage	Zero boil-off or cryogenless	Ideally, magnet cool-down should be possible without helium loss
Cryogenic system	Operation at 4.2 K or warmer	Large, complicated cryogenic facilities for recuperating and recycling helium are undesirable to reduce siting requirements and cost
Size and weight	As compact as possible	Simplifies transport and siting and makes the system more attractive for human subjects
Quench	No damage to the magnet; re-ramping the magnet should be straightforward	An emergency quench should reduce the residual magnetic field to a safe level compatible with ferromagnetic objects (approx. 20 mT [58]) as quickly as possible
Resistive shims	Roughly 950 Hz cm^{-1} and 120 Hz cm^{-2} for 1st and 2nd-order spherical harmonics at 14 T (see [59] for details and 3rd-order targets)	May be supplemented with multi-coil shimming. Resistive shim design is usually independent of magnet design
Gradients	$\geqslant$80 mT m^{-1} amplitude and $\geqslant$200 mT m^{-1} ms^{-1} switching speed for whole-body gradients	State-of-the-art whole-body gradients at 3 T provide 200 mT m^{-1}, which would be a more preferable target
Gradient-magnet interactions	Extremely important and challenging multi-physics problem requiring close interaction between magnet and gradient designers to avoid unintended magnet quenches	Resonant frequencies of magnet structures and gradient coil should be avoided during imaging
RF-magnet interactions	No interactions relevant to magnet design	

overly large. An incremental increase in field strength with judicious step sizes is preferable to ensure that subject safety can be adequately evaluated along the way to higher field strengths. Thus, the choice of 14 T as the next step in field strength progression appears to be very sensible.

3.1.2. Head-only vs. whole-body magnets. Another key specification is the size of the magnet opening that is required and ultimately the field of view available for imaging. Due to challenges in achieving homogeneous excitation of large objects at high RF frequencies (cf. section 3.4), much of the current research and clinical usage of UHF is focused on imaging of the head or small joints. Thus, it might be reasonable to pursue a system design that only provides an opening large enough for head-only imaging. Historically, there have been several head-only MR system designs, including at 3 T [61] and at 7 T [62].

Nevertheless, there are good arguments for pursuing a system that can accommodate the entire body, since

advancements in brain imaging can be extended to other body regions, which is of particular interest for clinical research, as many disease processes affect the torso. Thus, a much broader research community can be accommodated by a whole-body system. A UHF or EHF system would provide valuable insights into diseases involving organs outside the brain including diabetes, cardiovascular disease, fatty liver disease and cirrhosis, organ transplants, chronic kidney disease, and disorders of the reproductive system. A prime example is cancer: according to the current statistics in the United States [63], only 3% of cancer-related deaths are related to brain and other nervous system cancers. The vast majority of deaths are related to prostate, breast, colon, urinary bladder, uterine, kidney, and pancreas cancer, which can only be studied with a whole-body magnet. Even if physiological motion at highest spatial resolution hampers full leveraging of the benefits of UHF and EHF for conventional hydrogen-based imaging, this restriction does not extend to other nuclei such as deuterium, sodium, phosphorus, potassium, chlorine, and oxygen. These nuclei can only be imaged at low spatial resolution if at all at lower field strengths due to limited sensitivity. Because of the limited sensitivity, the full potential of these nuclei for metabolic imaging has not yet been fully exploited [64]. For these reasons, both the 14 T MR initiative in the Netherlands [23] and Germany [20] support pursuing a whole-body magnet.

The outer diameter of head-only gradients requires a warm-bore opening of the magnet on the order of 65–70 cm [62]. Whole-body gradients, on the other hand, require a warm bore on the order of 80–90 cm [13, 14]. To minimize material requirements and cost, the warm bore of the magnet should be chosen to match the outer diameter of the gradient coil as closely as possible. However, due to interactions between the switching gradient fields and the conducting structures of the magnet [17, 65], which can lead to a magnet quench, it can be advantageous to enlarge the warm bore of the magnet (cf. section 3.3.1). At 3 T, a very compact magnet design has been introduced for head imaging with a warm bore of 62 cm [61]; this is probably the smallest magnet diameter reasonable for an EHF system if head and extremity imaging are sufficient.

3.1.3. Magnetic field homogeneity. In the view of MR imaging and spectroscopy, magnetic field inhomogeneities occur in two spatial domains. Microscopic or mesoscopic field variations in the range of micrometers, for example within a capillary network, generate a certain contrast in $T2^*$- or T2-weighted images, or a broadening of resonances in localized spectroscopy. Macroscopic field changes in the range of centimeters are produced by the main magnet itself, and by local magnetization of tissues with different susceptibility and shape. These field variations generate spatial image distortions, signal voids, blurring, and many more disadvantageous effects. In general, the main magnet is designed to provide a certain field homogeneity within a specified volume. Additional field distortions induced by individual tissue configurations are partially compensated with a set of shim coils, as described in section 3.2.

Despite high efforts in the manufacturing process, a new magnet leaving the factory will typically have a magnetic field inhomogeneity in the range of ∼500 ppm (peak–peak) over the maximum imaging volume. Due to local variations in the building structure (e.g. steel reinforcements), the field homogeneity of the magnet has to be refined during the on-site system installation. On-site shimming is usually performed with passive shims (pieces of iron of defined weight and shape or ferromagnetic pellets are placed at precalculated positions) and/or with superconducting shims (cf section 3.2.1). This shimming is performed during installation of the magnet and is fixed, so it cannot be altered on a per-patient basis.

For a typical 1.5 T clinical system, field homogeneities of about 0.1 ppm (volume root-mean-square) within a spherical volume of 30 cm can be achieved. Current UHF installations (7 T, 9.4 T, 10.5 T, and 11.7 T) provide field homogeneities on the order of 0.03–0.1 ppm within a 30 cm sphere. This field homogeneity is already about a factor of 5–20 better compared to the field distribution within a human head induced by the diamagnetism of tissue and the paramagnetism of air cavities and bone structures, which amounts to about 0.5–2 ppm. In this respect, a further improvement in magnet homogeneity is less important than a dedicated shim system that allows further refinement for each individual patient and body region, as described in section 3.2.

3.1.4. Short-term and long-term magnet stability. One aspect of stability requirements is the duration over which the stability is quantified: short-term stability refers to the interval over which the system does not adjust the center frequency assumed for MR measurement, which could be the entire duration of a subject examination, but might be much shorter if the system adjusts the center frequency for each imaging sequence or even within individual imaging sequences. Long-term stability refers to a much longer time period, determined by the time between two ramping procedures of the magnet to stay within the design frequency bandwidth of the RF subsystem.

When examining stability requirements, a main question is relative (ppm) vs. absolute (Hz) frequency drift at different field strengths. For some applications, relative drift is relevant (e.g. for field mapping). For others, such as MR spectroscopy (MRS), the line width sets a limit to the field drift and thus the drift requirement depends on the homogeneity. If the homogeneity at different fields is similar in relative terms, the spectral lines will get absolutely broader in Hz; if it is similar in absolute terms, the lines will get relatively narrower as main magnetic field increases. Field drift needs to be small relative to the line width for MRS to fully benefit. For many phase-based methods (QSM, flow) and multi-shot acquisitions, the acceptable phase variation within the desired echo time is relevant. In EPI, for example, field drift will lead to a spatial shift in the reconstructed image as the effective imaging bandwidth is very small in the phase-encoding direction. For high resolution EPI it can be as low as 50 Hz pixel^{-1}.

It should be noted that short-term magnetic field variation can also be caused by thermal effects, e.g. due to gradient-induced heating of magnet or shim components. This effect

Table 2. Long-term stability of seven UHF magnets in the GUFI network, averaged over several years of operation [68].

Site	Magnet Type	Drift (Hz d^{-1})
1	7 T, 90 cm warm bore, passively shielded	−0.01
2	7 T, 90 cm warm bore, passively shielded	−0.18
3	7 T, 90 cm warm bore, passively shielded	−0.7
4	7 T, 90 cm warm bore, passively shielded	−94
5	7 T, 90 cm warm bore, passively shielded	−220
6	7 T, 83 cm warm bore, actively shielded	−1.4
7	9.4 T, 90 cm warm bore, passively shielded	−10

can dominate the short-term magnetic field stability and it is not caused by a current loss in the superconducting magnet coils.

Most of these effects can be corrected if the field drift is accurately measured. Thus, the question is whether the magnetic field needs to be inherently temporally stable or if accurate supervision would suffice. Compensation of field drift is routinely done as part of a calibration that is performed whenever a new patient or object is placed into the magnet by measuring the Larmor frequency of the protons. An important part of the calibration for imaging is locking onto the correct peak in the resonance spectrum, either water or fat or another desired peak. Depending on the software, this calibration may, however, only be performed once at the commencement of a new examination as long as the same anatomical region remains in the center of the magnet. Any frequency shifts over the duration of the examination would be missed. There are, however, also techniques to adjust the center frequency in real-time during the acquisition based on data collected as part of the imaging sequence [66]. An alternative would be to monitor the field drift with independent hardware such as a field camera using, for example, ^{19}F probes not visible in conventional images [67].

Regular quality control measurements within the German Ultrahigh Field Imaging (GUFI) network [68] revealed that even for persistent 7 T and 9.4 T superconducting magnets, the downward field drift can be as high as 220 Hz d^{-1} (table 2). It is standard procedure to periodically ramp the magnets up when the center frequency falls out of the bandwidth of the RF system (e.g. ±500 kHz), but this is undesirable if required too often, as it necessitates system downtime. In the case of the 7 T system in table 2 with a drift of 220 Hz d^{-1}, it was necessary to ramp the magnet about once every eight years, which was acceptable. Regarding short-term stability, over a 1 h examination the field of this system might drift on the order of 10 Hz (0.033 ppm h^{-1}), which would only be of concern for a subset of applications such as spectroscopy, and only if the center frequency is not adjusted during the exam duration.

This opens up a rather general question about system performance: do we need to invest in extensive engineering to design a super-stable magnet or is it adequate to relax the requirements as long as any spatial or temporal variation is accurately measured at the cost of increased system complexity. For EHF systems, the solution may be a combination of both to ensure that the signal does not drift too much and stays in the detectable range for extended periods, but within that range can be corrected on the basis of sensor information. The design specification of the Iseult 11.7 T magnet was 0.05 ppm h^{-1} [17], which should be sufficient for most applications without additional compensation, and should be sufficient for even the most demanding use cases if additional measures such as sensor feedback are implemented.

3.1.5. Other magnet considerations. In addition to the aforementioned primary specifications, there are a number of secondary specifications that should be discussed and agreed upon as part of a UHF or EHF magnet design. From the perspective of MRI scientists, some of these specifications may not be absolute, rather the targets will be set to achieve 'as good as possible' within economic constraints. If all other factors remain constant, the MRI users will prefer a design that minimizes or maximizes one of these particular parameters (e.g. minimization of magnet weight or required passive shielding).

As already mentioned above, one consideration is whether the residual resistance in the joints of the superconductor is low enough to support persistent operation. Although almost all clinical systems operate in the persistent mode, a driven magnet with a permanently attached power supply should be acceptable as long as field drift is limited (cf section 3.1.4). The human 11.7 T system in Paris, for example, operates in the driven mode [18]. At thermal equilibrium, field stability of approximately 3 ppb h^{-1} has been reported, which is well below the design target of 50 ppb h^{-1} [17]. For comparison, the previously mentioned stability of a persistent 7 T system within the GUFI network of 220 Hz d^{-1} translates to 30 ppb h^{-1} .

Another important design consideration is whether the magnet should be actively or passively shielded. The first generation of 7 T systems were passively shielded, an approach that was chosen to reduce project risk. Later, actively shielded 7 T systems were introduced [14]. Although almost all current clinical MRI systems are actively shielded, any project targeting a field strength >12 T would likely pursue installation at a greenfield site, where the larger stray fields can be accommodated. Interestingly, the Paris 11.7 T system is actively shielded, a design choice that was made owing to siting constraints [17]. The 14 T HTS magnet planned for Nijmegen will be passively shielded, but due to the extreme compactness of the magnet,

the stray field is very similar to a passively-shielded 7 T magnet made with NbTi [24].

Given the huge increases in liquid helium prices as well as the several episodes of helium shortages in recent years [69], a further goal should be minimization of helium usage. This includes minimizing the amount of helium required for initial cool down and commissioning of the magnet as well as the amount lost to boil off during operation. Several projects have experienced significant delays because they could not acquire the large volume of helium needed to put the magnet into operation. A reasonable design should utilize other means for most of the cool down, such as incorporating additional cryocoolers to achieve cooldown between liquid nitrogen temperature (77 K) and the end operating temperature [14], even if this means that the commissioning phase takes longer. The first generation of 7 T magnets were not zero boil-off, but later designs have addressed this weakness [14]. The 14 T system for Nijmegen is even intended to be cryogenless [24], but a zero boil-off design should be sufficient for most EHF projects at $>$12 T considering the uniqueness of these systems.

During operation, any cryogenic system utilized for the system should be reliable and easy to maintain. MRI magnets at conventional field strengths typically operate at 4.2 K, which is a well-established technology [12]. Above about 9.5 T, the material parameters of NbTi are insufficient to operate at 4.2 K, requiring lower operational temperatures, which can be achieved by pumping the magnet to lower the pressure. Such super-chilled cryogenic systems are more complicated, require more space, and can increase helium usage; the magnets are also more likely to quench due to lower thermal stability [12]. Magnet designs that utilize alternative superconductors such as Nb_3Sn or HTS can be operated at 4.2 K even at much higher field strengths than 9.5 T due to the higher critical magnetic field at liquid helium temperatures compared to NbTi.

All other things being equal, MRI scientists will prefer a design that is compact and light. On the one hand, this will simplify siting issues and make it easier to identify and finance a suitable location for the magnet room, and it will simplify transport of the magnet from the site of manufacture to the installation site. On the other hand, a compact design will be more attractive to volunteers and patients who are to be examined in the system. To achieve a compact design, generally high current density is desirable in the superconducting material. Since the critical current density falls with increasing field strength, the superconductor choice depends on the targeted field strength. The National High Magnetic Field Laboratory in the USA has generated preliminary design parameters for a 20 T head-only MRI magnet based on Nb_3Sn, but the authors pointed out that the potential higher current density of HTS at 20 T could further reduce the magnet size if this superconductor technology matures sufficiently [70]. The 11.7 T whole-body system in Paris with a warm bore of 90 cm is based on NbTi superconductor, which needs to be supercooled to 1.8 K to achieve sufficient current density. It is also actively shielded, which significantly increases its girth [71]. The cryostat of the magnet is 5.2 m long with a diameter of 5 m, and the weight of the magnet is 132 tons [72]. To ship the completed magnet from the factory to its final home, transport by heavy-load truck, barge, and boat was necessary [71]. The 14 T system being planned in Nijmegen is based on HTS, passively shielded, and has a warm bore of only 82 cm, allowing it to be much more compact. It is planned to be 2.6 m long, 1.4 m in diameter, and weigh 16 tons, making siting and transport much more flexible [23].

An important safety consideration for human magnet designs is the ability to quickly and safely quench the magnetic field in an emergency. Due to the large stored energy in UHF/EHF magnets, proper magnet design should incorporate adequate quench protection to prevent damage to the magnet due to overheating or voltage spikes. Liquid helium will be converted to a large volume of gas that needs to be safely vented from the magnet room. Several systems at 7 T, 9.4 T, and 11.7 T have suffered damage during a quench (both spontaneous and intentional) that prevented the magnet from being re-ramped. The subsequent repairs were both extremely costly and time intensive. Such downtime should be avoided through appropriate design if at all possible.

3.2. Shims

To further refine the uniformity of the main magnetic field during installation, either superconducting shims as part of the magnet itself or additional passive shims may be utilized [12]. Passive shims are usually small iron pieces that are placed in the warm bore of the magnet and magnetized by the main magnetic field; since they are fully saturated even at fairly low magnetic fields, their relative efficiency decreases as the field strength increases [12]. Resistive shims that can be adjusted for each volunteer or patient are mainly used to compensate for field inhomogeneities within tissue induced by tissue susceptibility differences and shape. Most of these inhomogeneities are static, but time-varying field fluctuations arising from physiological processes such as respiration require an adaptive and real-time update of shim currents.

3.2.1. Superconducting shims. Superconducting shims are used to improve the main magnetic field homogeneity (sometimes in combination with passive shims) and are adjusted during the system installation and tune-up. However, these shims cannot be changed dynamically and thus cannot be used for object-specific shimming. It has been reported for the 11.7 T system at NeuroSpin that magnetic coupling between the superconducting shims and the main magnet coil could cause activation of the magnet monitoring system and discharge of the magnet in some failure modes, so that the system currently relies solely on passive shims for achieving homogeneity targets [17].

3.2.2. Resistive shims. Most shim systems consist of resistive copper coils either integrated within the gradient coil system or mounted locally close to the subject. These coils generate a superposition of field distributions to compensate for field inhomogeneities within the object. However, external

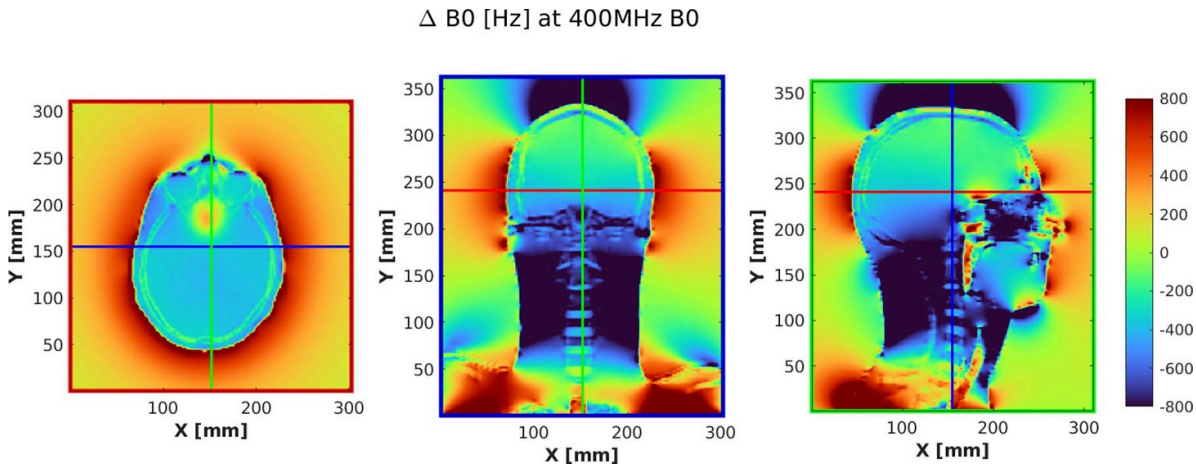

Figure 4. Simulated field deviation in Hz at a main field of 9.4 T for the Duke body model from the Virtual Family library [74]. Figure courtesy of D. Bosch, Max Planck Institute for Biological Cybernetics, Tübingen.

magnetic fields can only fully compensate for field inhomogeneities within the object if the object does not contain any source of magnetic field, which, for example, is not the case for the human head [73]. Figure 4 shows an example of a simulated magnetic field distribution (in frequency units) within and around a human brain at 9.4 T without applying any shim compensation.

As this frequency pattern scales linearly with the main magnetic field, the currents through the shim coils to partially compensate for these inhomogeneities also need to increase linearly with field strength. Depending on the efficiency of the shim coils (generated magnetic field/current), existing shim amplifiers used at 3 T provide currents in the range of 10–20 A per channel, so at 14 T currents of about 50–100 A are required if similar shim coils are used. In terms of absolute capability, a recent paper examining B_0 shimming with spherical harmonics for single-voxel spectroscopy in the human brain recommended 200 Hz cm^{-1} for the 1st-order shims and 15–25 Hz cm^{-2} for the 2nd-order shims at 3 T [59]. Since susceptibility-induced distortions scale with field strength, this would imply 933 Hz cm^{-1} and 70–117 Hz cm^{-2} at 14 T [59]. They also provide recommendations for each 3rd-order term.

One main advantage of resistive shimming over passive and superconducting shimming is that the currents through resistive shims can be changed dynamically. This allows shimming to be performed on a subject-by-subject basis, or even dynamically on a slice-by-slice basis within the same subject during image acquisition [75]. In addition to static field deviations as shown in figure 4, dynamic field changes arising from physiological processes such as the movement of the chest wall, the changing volume and oxygenation of air in the lungs, and changes in blood oxygenation over the breathing cycle pose an even greater challenge. Both static and dynamic absolute field deviations increase linearly with the main magnetic field.

3.2.2.1. Spherical harmonics. Many MRI manufacturers implement shim coils based on spherical harmonic functions of various orders [76]. The mathematical foundation is based on the solution of Laplace's equation, $\nabla^2 B = 0$, which is derived from Maxwell's equations in regions with no current sources. Shim coils integrated into the gradient coil typically generate magnetic field patterns composed of a superposition of spherical harmonics up to 2nd order (mean frequency, *X, Y, Z, ZX, ZY, XY,* $X^2 - Y^2$, Z^2) and some channels of 3rd order. While 1st and 2nd-order spherical harmonic terms are effective at removing the lowest spatial order variations (which are the strongest ones), higher order spherical harmonics are required to compensate for more localized field deviations.

3.2.2.2. Multi-coil shimming. As shown in figure 4, the magnetic field inhomogeneities arising from the human anatomy can be highly localized, and compensation of these fields is not always optimally solved with a superposition of a limited number of spherical harmonic functions. In contrast, multi-coil (or matrix coil) shimming uses an array of local shim coils placed close to the sources of magnetic field perturbation to obtain the high spatial order field patterns needed to cancel the spatially localized field variations. Multi-coil shim coils are typically a set of simple loop geometries mounted on a supporting structure [77]. Juchem *et al* could demonstrate that a 48-channel system consisting of 4.7 cm loops arranged in four rings on an elliptic cylinder can in principle outperform global 1st–5th order spherical harmonic shimming [78]. Since both local matrix shim coils as well as RF transmit and receive coils need to be placed close to the target anatomy to maximize efficiency, potential coupling between RF and shim coils has to be minimized, for example with RF shields or traps [79].

At EHF, it is likely that a combination of spherical harmonic shim coils incorporated into the gradient coil as well as multi-coil shimming as part of a local shim array built into the RF coil or otherwise placed close to the target anatomy will be required to achieve optimum results, particularly in the brain and neck.

3.3. Gradients

Historically, gradient development and performance improvements have often been driven by specific applications. For example, fast measurement of contrast-enhanced angiography benefitted dramatically from fast switching gradients in the 1990s and became a clinical routine tool. This also allowed broader application of single-shot echo planar imaging, as shorter echo spacing became feasible. More recently, gradient amplitudes have been at the focus of development in order to reduce echo times, in particular for diffusion-weighted imaging, leading even to unique connectome MR systems and to much enhanced gradient amplitude in commercial 3 T MR. Research systems offer a combination of very high gradient slew rate and amplitude at 3 T and 7 T [55, 80, 81]. At very high magnetic field strength, T2 and T2* become shorter and, thus, shorter echo times and faster readout are not only desired but can increase signal even more than at lower field. High performance gradients will thus improve certain applications or make them feasible at very high field, while a number of standard imaging methods will be fully feasible even with 'conventional' gradients. The adoption of high-performance gradients at higher field strength requires handling not only acoustic noise, as the Lorenz forces increase linearly with field strength, but also magnet-gradient interactions that can transfer critical amounts of energy into the magnet structure (cf section 3.3.1).

A number of gradient design choices have to be made that impact one another. Gradient geometry, in particular outer and inner diameter, sets the main boundaries for application of the system. While the outer diameter is mainly given by the magnet bore, the inner diameter determines whether the system can be used for whole-body or head-only application. Whole-body gradients require an inner diameter of at least 60 cm, leading to a useable bore size of about 56 cm. However, clinical MRI systems have utilized 60 cm as the industry standard patient opening since the 1990s, and a patient bore diameter of at least 60 cm will be the most common specification for a whole-body system. Head-only gradients have been built with inner diameters down to 36 cm, but the accommodation of a separate multichannel transmit and receive RF coil may require somewhat more space. Smaller diameter gradients can deliver much higher performance. For modern gradient designs and power amplifiers, peripheral nerve stimulation sets the performance limit. If the wire pattern is co-designed with peripheral nerve stimulation thresholds, the applicable slew rate and amplitude can be significantly increased [82].

A 14 T or other EHF MRI system will certainly be functional and provide fertile ground for research studies even with conventional gradient performance (amplitude $\geqslant$80 mT m^{-1} and slew rate $\geqslant$200 mT m^{-1} ms^{-1} for whole-body gradients). Replacement by a high-performance gradient set at a later stage is always possible (200 mT m^{-1} for whole-body gradients), which would in particular benefit diffusion imaging applications.

3.3.1. Gradient-magnet interactions. Although the gradient coil is mounted inside the magnet warm bore and typically secured by mechanical wedging, requiring no direct electrical interfaces to the magnet, proper consideration of interactions between the gradients and the magnet are critical during the design phase to ensure that the switching magnetic fields of the gradients will not induce an unwanted quench. Modern gradient coils incorporate an active shielding layer on the outside of the primary coil windings to reduce magnetic field changes external to the coil and restrict field changes to the imaging volume within the coil. Despite optimization, current gradient coils will nevertheless generate eddy currents in the conducting components of the magnet such as the helium vessel, thermal shields, coil formers, and cryostat, dumping energy into the magnet and leading to heating. The oscillating magnetic fields will also induce mechanical vibrations, particular in thin structures like thermal shields inside the cryostat. Mechanical vibrations of the gradient coil itself can also be directly coupled to the inner bore of the magnet through the mounting hardware. Since mechanical vibration intensity increases with the static magnetic field, gradient-magnet interactions are more critical in UHF and EHF systems [83]. Any mechanical resonances of either the gradient coil or the magnet structure should be avoided by design measures or by excluding these frequencies from being generated in the imaging sequences [17, 83]. It is common practice to define forbidden parameter intervals in MRI pulse sequences to avoid critical frequencies. To reduce helium loss, it is in particular critical to understand the vibrational characteristics of the thermal shields, since the boil-off rate is highly dependent on vibrational amplitude and thus frequency [83]. UHF systems can lose their helium reserve within just a few hours of imaging at a critical frequency. Even modern clinical MRI systems that are nominally zero boil-off can lose helium if gradient switching occurs in a critical range.

The cryogenic system of the magnet must be conceived to distribute and dissipate any heating sufficiently quickly to avoid loss of superconductivity. These interactions should be thoroughly simulated and addressed with measures such as a larger helium bath, additional cryocoolers, or utilization of a superconducting material with a greater headroom between operating temperature and critical temperature [24, 60, 84]. A magnet constructed of NbTi operating at 11.7 T and 1.8 K will have lower thermal margin than a magnet operating with either Nb_3Sn or HTS at a field strength of 14 T and 4.2 K due to the improved superconductor properties [12].

The switching of the gradient fields inside the strong static magnetic field will also lead to mechanical vibrations. On the one hand, these vibrations will produce acoustic noise that can exceed 100 dB. The IEC 60 601-2-33 norm specifies that the maximum A-weighted RMS sound pressure level must not exceed 99 dBA [58]. On the other hand, the vibrations also cause vibration of the magnet itself [83], leading to electric fields in the cryostat and Joule heating [17].

Although significant advances have been made in modeling and simulating gradient-magnet interactions [83], experimental investigation of the final system is always required to identify resonances for each gradient axis where heating load is high [17]. It is possible to prevent gradient switching in critical frequency bands via software-programmable lockouts when selecting imaging parameters.

3.4. RF electronics

Since the RF resonance frequency in MR is proportionally coupled to the magnetic field strength via the MR condition, the static magnetic field strength of an MR system dictates the associated resonance frequency and thus the main frequency of the transmit/receive RF system and associated RF coils. Beyond this physical dependency there is no other significant direct interaction between the RF system components and the magnet components, so the magnet design does not depend as directly on this subsystem as on the gradient subsystem.

4. Known and potential risks of higher magnetic fields

MR is considered non-invasive and 'safe' if the limits regarding electromagnetic exposure are observed and good practice is employed in the exclusion of subjects with contraindications (e.g. non-suitable metallic or electronic implants). Currently, European and international guidelines (EU Directive, ICNIRP, FDA, and SCENIHR) do not consider exposure to static magnetic fields up to 7 or 8 T to be a significant risk for human subjects. For field strengths >8 T safe operation has to be established, while exposure to RF and gradients can stay within the current guidelines. Since the regulatory limits for exposure to both gradient magnetic fields and RF are unchanged at UHF and EHF, below we consider areas of interactions between the static magnetic field of MR and human tissue or implants that may become more critical with rising magnetic field strength. Although these interactions will not be the main concern of magnet designers, this information is of indirect interest, since these factors place limits on the ultimate useable magnetic field strength (cf. Table 1), whereby physiological effects are relevant for all study populations and implants are of particular significance for patient populations.

4.1. Tolerance of human subjects to UHF and EHF magnetic fields

The ultimate concern when performing MRI examinations in humans is the safety of both the subjects under examination as well as the involved workers. Regarding the static magnetic field, the generally accepted upper limit as provided in the industry norm IEC 60601-2-33 is currently 8 T for both patients and workers (cf [58] and the rationale therein). For values above 8 T, the system will operate continuously in the second level controlled operating mode, which in most countries requires dedicated approval, for example from an ethics committee or institutional review board.

When considering exposure to the magnet of an MRI system, scenarios must consider not only the static value of the field but also the effect of time-varying fields induced by motion through the field of the magnet [85–87]. In terms of physiologic effects on humans, numerous possible mechanisms or possible observable effects have been postulated. These include impeded nerve conduction, cardiac stimulation, higher blood pressure due to electrical blood conductivity, carcinogenic effects, teratogenicity, chromosome aberrations, DNA strand breaks, reproductive impairment, hearing loss due to acoustic noise generated by interactions with the gradient magnetic fields, and impairments to brain cognitive function and motor control [88–90].

Data for human exposure to high magnetic fields is currently only available up to 10.5 T [91], but similar data for 11.7 T are expected to be available shortly. None of the available human data have revealed any significant physiologic changes such as substantially elevated heart rate or blood pressure. Nevertheless, several transient effects such as vertigo, nystagmus, metallic taste, nausea, and magnetophosphenes have been observed. These effects may occur at lower field strengths, but they start to affect an increasing number of subjects at or above 7 T [92]. At some point, even if the effects are only transient and not harmful, they may impede acceptance of higher magnetic fields by human subjects.

The common model for explaining vertigo and nausea is an interaction between motion-induced or innate currents and the sensory organs of the inner ear. Lorentz forces acting on the ionic currents in the cupula can induce nystagmus even when lying still [93, 94]. The disconnect in sensory input between the vestibular, the proprioceptive, and the visual systems is sufficient to induce nausea and vertigo, similar to motion sickness. At 7 T, it has been shown that the effects can be ameliorated by the administration of motion sickness medication such as diphenhydramine [95]. A less invasive approach is to optimize the angle between the static magnetic field and the ionic currents of the ear to minimize interaction [96]. The latter study found that the weakest effects are observed in the supine position when the plane formed by the external auditory canals and the lower orbital margins is tilted approximately 20 degrees forward of vertical.

At static magnetic fields higher than 10.5 T, only animal data are available. After exposure, a common observation in mice and rats is circling behavior either when walking or swimming [97, 98]. However, in most studies, any behavior anomalies resolve within several tens of minutes after exposure [99, 100]. In a recent study at 16.4 T, the circling in mice was persistent for several weeks post-exposure [101]. A separate group exposed to 10.5 T did not show this behavior. Methodologically, an important difference between this study and others was that the mice were free to roam inside the 16.4 T field during exposure. A similar study performed at 17.2 T but with fixated animals did not reveal any long-lasting behavioral effects [102]. That study also specifically tested auditory brainstem response and did not find any evidence for damage to the cochlear hair cells.

Although in human MRI examinations the subjects will remain relatively stationary within the magnetic field, further animal studies are necessary to fully understand possible interactions with the vestibular system and verify whether any permanent damage might occur.

4.2. Implants

UHF and EHF MRI systems with magnetic field strengths above 7 T are initially intended for research purposes, providing no direct benefit to individual participants. In this context,

a risk-benefit analysis does not support including subjects with implants that may pose safety risks due to interactions with the electromagnetic fields of the system, particularly the higher static magnetic field and RF excitation fields. However, there is a societal benefit from these research investigations, meaning the risk does not need to be reduced to zero. Even for participants without implants, the risk of any MR examination is never zero.

Similar to the early developments at 7 T, we expect exclusion criteria to be very strict for any new magnetic field strength but to become more relaxed as experience is gained. Scientific investigations will determine the extent of implant interactions and provide approaches to mitigate any risks. This research is crucial to ensure that the benefits of EHF can be extended to a broader segment of the population, especially as the number of people with implants has dramatically increased in the past two decades, and the global market and the variety of implants continue to grow. Therefore, unlike the early 7 T scenario where implants received minimal attention for many years, implants should be a key consideration in all EHF MRI projects from the outset. The objective is to swiftly remove as many as possible from the exclusion criteria while maintaining safety.

With regard to the strong magnetic fields of EHF MR systems, potential interaction with metallic implants is a major safety concern. Objects and implants made of ferromagnetic materials may be subject to significant magnetic force and torque when brought near to an MR system. Fortunately, the majority of small and passive metallic implants such as dental implants, vascular stents, surgical screws, clips, etc. are made of non-ferromagnetic materials, and magnetic attraction and torque do not apply here. Consequently, in these cases it does not matter whether the subject with such implants is investigated at 1.5 T, 3 T, or in a UHF or even EHF MR system, although the absence of forces/torques should be verified at each new field strength to exclude residual ferromagnetics in alloys or due to surface impurities introduced during machining of the materials [103].

Even for completely non-magnetic metallic implants, RF heating may be of potential concern because they are electrically conducting. However, when such implants are located far enough away from the local RF transmit coil during an UHF/EHF MRI examination, an exam might be admissible since no excessive RF heating is then to be expected. The conditions under which safe examinations can be performed, however, need to be established for each new magnetic field strength due to the increasing RF frequency.

5. Conclusion

The history of human MRI is characterized by the utilization of ever-higher static magnetic fields as technology has progressed and the safety of each new field strength has been established. This trend will continue moving forward, raising a standing challenge to magnet researchers and developers. In particular, the technological limits of NbTi have been reached with the implementation of several 11.7 T human-sized magnets based on solenoid or double-pancake designs. Currently, a double-pancake 14 T system is under construction based on an HTS ReBCO superconductor. Given the as-yet-unknown physiological effects and concomitant safety questions related to human exposure to such high magnetic fields, a stepwise progression in field strength is prudent, allowing these open questions to be investigated and resolved. Nevertheless, as soon as the transition to a new superconductor technology beyond NbTi is achieved, the path forward to even higher magnetic fields such as 16.4 T (700 MHz) for human MRI will be unlocked.

Data availability statement

No new data were created or analysed in this study.

Acknowledgments

The authors wish to thank David Feinberg of the University of California Berkeley for providing figure 2, Philip Boyd of the German Cancer Research Center in Heidelberg for providing figure 3, and Dario Bosch of the Max Planck Institute for Biological Cybernetics in Tübingen for providing figure 4.

Funding

Klaus Scheffler received funding from ERC Advanced Grant, Grant/Award Number: 834940.

Ethical statement

No work requiring ethical review was performed in this study.

Authors' contribution

All authors drafted various sections of the manuscript. All authors were responsible for critical revision of the final version.

ORCID iDs

Mark E Ladd https://orcid.org/0000-0002-4128-9440
Klaus Scheffler https://orcid.org/0000-0001-6316-8773
Oliver Speck https://orcid.org/0000-0002-6019-5597

References

[1] Bloch F 1946 Nuclear induction *Phys. Rev.* **70** 460–74
[2] Purcell E M, Torrey H C and Pound R V 1946 Resonance absorption by nuclear magnetic moments in a solid *Phys. Rev.* **69** 37–38
[3] Hahn E L 1950 Spin echoes *Phys. Rev.* **80** 580–94
[4] Ernst R R and Anderson W A 1966 Application of Fourier transform spectroscopy to magnetic resonance *Rev. Sci. Instrum.* **37** 93–102

[5] Damadian R 1971 Tumor detection by nuclear magnetic resonance *Science* **171** 1151–3

[6] Lauterbur PC 1973 Image formation by induced local interactions: examples employing nuclear magnetic resonance *Nature* **242** 190–1

[7] Garroway A N, Grannell P K and Mansfield P 1974 Image formation in NMR by a selective irradiative process *J. Phys. C: Solid State Phys.* **7** L457–62

[8] Barfuss H, Fischer H, Hentschel D, Ladebeck R and Vetter J 1988 Whole-body MR imaging and spectroscopy with a 4-T system *Radiology* **169** 811–6

[9] Uğurbil K 2018 Imaging at ultrahigh magnetic fields: history, challenges, and solutions *Neuroimage* **168** 7–32

[10] Schmitt F, Grosu D, Mohr C, Purdy D, Salem K, Scott K T and Stoeckel B 2004 3 Tesla MRI: successful results with higher field strengths *Radiologe* **44** 31–47

[11] Khan B A and Siegel E L 2021 Could very low field strength be the next frontier for MRI? (available at: www.diagnosticimaging.com/view/could-very-low-field-strength-be-the-next-frontier-for-mri-) (Accessed 7 August 2024)

[12] Parizh M and Stautner W 2022 MRI Magnets *Handbook of Superconductivity* (CRC Press) pp 437–92

[13] Robitaille P M *et al* 1999 Design and assembly of an 8 tesla whole-body MR scanner *J. Comput. Assist. Tomogr.* **23** 808–20

[14] Warner R 2016 Ultra-high field magnets for whole-body MRI *Supercond. Sci. Technol.* **29** 094006

[15] Sadeghi-Tarakameh A *et al* 2020 In vivo human head MRI at 10.5T: a radiofrequency safety study and preliminary imaging results *Magn. Reson. Med.* **84** 484–96

[16] He X *et al* 2020 First in-vivo human imaging at 10.5T: imaging the body at 447 MHz *Magn. Reson. Med.* **84** 289–303

[17] Boulant N and Quettier L Iseult Consortium 2023 Commissioning of the Iseult CEA 11.7 T whole-body MRI: current status, gradient-magnet interaction tests and first imaging experience *MAGMA* **36** 175–89

[18] Quettier L *et al* 2020 Commissioning completion of the iseult whole body 11.7 T MRI system *IEEE Trans. Appl. Supercond.* **30** 1–5

[19] CEA 2024 A world premiere: the living brain imaged with unrivaled clarity thanks to the world's most powerful MRI machine *From Research to Industry* (available at: www.cea.fr/english/Pages/News/world-premiere-living-brain-imaged-with-unrivaled-clarity-thanks-to-world-most-powerful-MRI-machine.aspx) (Accessed 17 April 2024)

[20] Ladd M E *et al* 2023 Germany's journey toward 14 Tesla human magnetic resonance *MAGMA* **36** 191–210

[21] The Wire 2022 University of Nottingham awarded £29 million for UK's most powerful MRI scanner (West Bridgford Wire) (available at: https://westbridgfordwire.com/university-of-nottingham-awarded-29-million-for-uks-most-powerful-mri-scanner/) (Accessed 21 August 2022)

[22] UK UHF MR Research Community *Proposed national facility for 11.7T human MRI scanning* (University of Nottingham) (available at: www.nottingham.ac.uk/research/groups/spmic/research/national-facility-for-ultra-high-field-11.7t-human-mri-scanning/index.aspx) (Accessed 21 August 2022)

[23] Bates S *et al* 2023 A vision of 14 T MR for fundamental and clinical science *MAGMA* **36** 211–25

[24] Li Y and Roell S 2021 Key designs of a short-bore and cryogen-free high temperature superconducting magnet system for 14 T whole-body MRI *Supercond. Sci. Technol.* **34** 125005

[25] Xu A *et al* 2021 Experimental research of the new developed High-Jc Nb3Sn superconducting strand for 14 T MRI magnet *IEEE Trans. Appl. Supercond.* **31** 1–4

[26] Wang Y, Wang Q, Wang H, Chen S, Hu X, Liu Y and Liu F 2021 Actively-shielded ultrahigh field MRI/NMR superconducting magnet design *Supercond. Sci. Technol.* **35** 014001

[27] Pohmann R, Speck O and Scheffler K 2016 Signal-to-noise ratio and MR tissue parameters in human brain imaging at 3, 7, and 9.4 tesla using current receive coil arrays *Magn. Reson. Med.* **75** 801–9

[28] Le Ster C *et al* 2022 Magnetic field strength dependent SNR gain at the center of a spherical phantom and up to 11.7T *Magn. Reson. Med.* **88** 2131–8

[29] Guérin B, Villena J F, Polimeridis A G, Adalsteinsson E, Daniel L, White J K and Wald L L 2017 The ultimate signal-to-noise ratio in realistic body models *Magn. Reson. Med.* **78** 1969–80

[30] Pfrommer A and Henning A 2018 The ultimate intrinsic signal-to-noise ratio of loop- and dipole-like current patterns in a realistic human head model *Magn. Reson. Med.* **80** 2122–38

[31] Nassirpour S, Chang P and Henning A 2018 High and ultra-high resolution metabolite mapping of the human brain using 1H FID MRSI at 9.4T *Neuroimage* **168** 211–21

[32] Korzowski A, Weckesser N, Franke V L, Breitling J, Goerke S, Schlemmer H-P, Ladd M E, Bachert P and Paech D 2021 Mapping an Extended Metabolic Profile of Gliomas Using High-Resolution 31P MRSI at 7T *Front. Neurol* **12** 735071

[33] Henning A 2018 Proton and multinuclear magnetic resonance spectroscopy in the human brain at ultra-high field strength: a review *Neuroimage* **168** 181–98

[34] Budinger T F *et al* 2016 Toward 20 T magnetic resonance for human brain studies: opportunities for discovery and neuroscience rationale *MAGMA* **29** 617–39

[35] Polenova T and Budinger T F 2016 Ultrahigh field NMR and MRI: science at a crossroads. Report on a jointly-funded NSF, NIH and DOE workshop, held on November 12–13, 2015 in Bethesda, Maryland, USA *J. Magn. Reson.* **266** 81–86

[36] Budinger T F and Bird M D 2018 MRI and MRS of the human brain at magnetic fields of 14T to 20T: technical feasibility, safety, and neuroscience horizons *Neuroimage* **168** 509–31

[37] Ladd M E, Bachert P, Meyerspeer M, Moser E, Nagel A M, Norris D G, Schmitter S, Speck O, Straub S and Zaiss M 2018 Pros and cons of ultra-high-field MRI/MRS for human application *Prog. Nucl. Magn. Reson. Spectrosc.* **109** 1–50

[38] Platt T, Ladd M E and Paech D 2021 7 Tesla and beyond *Invest. Radiol.* **56** 705–25

[39] Jones S E, Lee J and Law M 2021 Neuroimaging at 3T vs 7T: is it really worth it? *Magn. Reson. Imaging Clin. N. Am.* **29** 1–12

[40] Menon R G, Chang G and Regatte R R 2021 Musculoskeletal MR Imaging Applications at Ultra-High (7T) Field Strength *Magn. Reson. Imaging Clin. N. Am.* **29** 117–27

[41] Düzel E, Costagli M, Donatelli G, Speck O and Cosottini M 2021 Studying Alzheimer disease, Parkinson disease, and amyotrophic lateral sclerosis with 7-T magnetic resonance *Eur. Radiol. Exp.* **5** 36

[42] Weldon K B and Olman C A 2021 Forging a path to mesoscopic imaging success with ultra-high field functional magnetic resonance imaging *Phil. Trans.* R **376** 20200040

[43] Bloch K M, Guye M and Poser B A 2023 *Ultra-High Field Neuro MRI* (Elsevier)

[44] Gallichan D, Marques J P and Gruetter R 2016 Retrospective correction of involuntary microscopic head movement using highly accelerated fat image navigators (3D FatNavs) at 7T *Magn. Reson. Med.* **75** 1030–9

[45] Maclaren J *et al* 2012 Measurement and correction of microscopic head motion during magnetic resonance imaging of the brain *PLoS* **7** e48088

[46] Aranovitch A, Haeberlin M, Gross S, Dietrich B E, Wilm B J, Brunner D O, Schmid T, Luechinger R and Pruessmann K P 2018 Prospective motion correction with NMR markers using only native sequence elements *Magn. Reson. Med.* **79** 2046–56

[47] Lüsebrink F, Mattern H, Yakupov R, Acosta-Cabronero J, Ashtarayeh M, Oeltze-Jafra S and Speck O 2021 Comprehensive ultrahigh resolution whole brain in vivo MRI dataset as a human phantom *Sci. Data* **8** 138

[48] Yang J, Fan J, Ai D, Zhou S, Tang S and Wang Y 2015 Brain MR image denoising for Rician noise using pre-smooth non-local means filter *Biomed. Eng.* **14** 2

[49] Manjón J V and Coupe P 2018 MRI denoising using deep learning *Patch-Based Techniques in Medical Imaging* (Springer International Publishing) pp 12–19

[50] Moreno López M, Frederick J M and Ventura J 2021 Evaluation of MRI denoising methods using unsupervised learning *Front. Artif. Intell.* **4** 642731

[51] van der Zwaag W, Francis S, Head K, Peters A, Gowland P, Morris P and Bowtell R 2009 fMRI at 1.5, 3 and 7 T: characterising BOLD signal changes *Neuroimage* **47** 1425–34

[52] Han S, Son J P, Cho H, Park J-Y and Kim S-G 2019 Gradient-echo and spin-echo blood oxygenation level-dependent functional MRI at ultrahigh fields of 9.4 and 15.2 Tesla *Magn. Reson. Med.* **81** 1237–46

[53] Kuehn E and Sereno M I 2018 Modelling the human cortex in three dimensions *Trends Cognit. Sci.* **22** 1073–5

[54] Polimeni J R, Fischl B, Greve D N and Wald L L 2010 Laminar analysis of 7T BOLD using an imposed spatial activation pattern in human V1 *Neuroimage* **52** 1334–46

[55] Feinberg D A *et al* 2023 Next-generation MRI scanner designed for ultra-high-resolution human brain imaging at 7 Tesla *Nat. Methods* **20** 2048–57

[56] Zaiss M, Jin T, Kim S-G and Gochberg D F 2022 Theory of chemical exchange saturation transfer MRI in the context of different magnetic fields *NMR Biomed.* **35** e4789

[57] Windschuh J, Zaiss M, Ehses P, Lee J-S, Jerschow A and Regatte R R 2019 Assessment of frequency drift on CEST MRI and dynamic correction: application to gagCEST at 7 T *Magn. Reson. Med.* **81** 573–82

[58] International Electrotechnical Commission 2022 Medical electrical equipment-Part 2–33: particular requirements for the basic safety and essential performance of magnetic resonance equipment for medical diagnosis IEC 60601–2–33 Edition 4.0

[59] Juchem C, Cudalbu C, de Graaf R A, Gruetter R, Henning A, Hetherington H P and Boer V O 2021 B0 shimming for in vivo magnetic resonance spectroscopy: experts' consensus recommendations *NMR Biomed.* **34** e4350

[60] Parizh M, Lvovsky Y and Sumption M 2017 Conductors for commercial MRI magnets beyond NbTi: requirements and challenges *Supercond. Sci. Technol.* **30** 014007

[61] Foo T K F *et al* 2018 Lightweight, compact, and high-performance 3T MR system for imaging the brain and extremities *Magn. Reson. Med.* **80** 2232–45

[62] Kickler N, van der Zwaag W, Mekle R, Kober T, Marques J P, Krueger G and Gruetter R 2010 Eddy current effects on a clinical 7T-68 cm bore scanner *MAGMA* **23** 39–43

[63] Siegel R L, Giaquinto A N and Jemal A 2024 Cancer statistics, 2024 *CA Cancer J. Clin.* **74** 12–49

[64] Niesporek S C, Nagel A M and Platt T 2019 Multinuclear MRI at ultrahigh fields *Top. Magn. Reson. Imaging* **28** 173–88

[65] Niu C, Wang L, Wang Y, Zhai Y, Qu H, Liu Y and Wang Q 2020 Numerical analysis of eddy current induced by z-gradient coil in a superconducting MRI magnet *IEEE Trans. Appl. Supercond.* **30** 1–6

[66] Benner T, van der Kouwe A J W, Kirsch J E and Sorensen A G 2006 Real-time RF pulse adjustment for B0 drift correction *Magn. Reson. Med.* **56** 204–9

[67] Brunner D O, Dietrich B E, Çavuşoğlu M, Wilm B J, Schmid T, Gross S, Barmet C and Pruessmann K P 2016 Concurrent recording of RF pulses and gradient fields—comprehensive field monitoring for MRI *NMR Biomed.* **29** 1162–72

[68] Voelker M N, Kraff O, Pracht E, Wollrab A, Bitz A K, Stöcker T, Quick H H, Speck O and Ladd M E 2017 Quality assurance phantoms and procedures for UHF MRI − the German Ultrahigh Field Imaging (GUFI) approach *Proc. Annual Meeting ISMRM* (*Honolulu*) p 3912

[69] Kramer D 2023 Helium prices surge to record levels as shortage continues *Phys. Today.* **76** 18–20

[70] Bird M D, Dixon I R and Toth J 2015 Large, high-field magnet projects at the NHMFL *IEEE Trans. Appl. Supercond.* **25** 1–6

[71] Quettier L *et al* 2018 Manufacturing completion of the iseult whole body 11.7 T MRI system *IEEE Trans. Appl. Supercond.* **28** 1–4

[72] Vedrine P *et al* 2015 Iseult/INUMAC whole body 11.7 T MRI magnet *IEEE Trans. Appl. Supercond.* **25** 1–4

[73] Meneses B P and Amadon A 2022 Physical limits to human brain B0 shimming with spherical harmonics, engineering implications thereof *MAGMA* **35** 923–41

[74] Christ A *et al* 2009 The Virtual Family—development of surface-based anatomical models of two adults and two children for dosimetric simulations *Phys. Med. Biol.* **55** N23

[75] Morrell G and Spielman D 1997 Dynamic shimming for multi-slice magnetic resonance imaging *Magn. Reson. Med.* **38** 477–83

[76] Roméo F and Hoult D I 1984 Magnet field profiling: analysis and correcting coil design *Magn. Reson. Med.* **1** 44–65

[77] Juchem C, Nixon T W, McIntyre S, Rothman D L and de Graaf RA 2010 Magnetic field modeling with a set of individual localized coils *J. Magn. Reson.* **204** 281–9

[78] Juchem C, Umesh Rudrapatna S, Nixon T W and de Graaf R A 2015 Dynamic multi-coil technique (DYNAMITE) shimming for echo-planar imaging of the human brain at 7 Tesla *Neuroimage* **105** 462–72

[79] Aghaeifar A, Zhou J, Heule R, Tabibian B, Schölkopf B, Jia F, Zaitsev M and Scheffler K 2020 A 32-channel multi-coil setup optimized for human brain shimming at 9.4T *Magn. Reson. Med.* **83** 749–64

[80] Huang S Y *et al* 2021 Connectome 2.0: developing the next-generation ultra-high gradient strength human MRI scanner for bridging studies of the micro-, meso- and macro-connectome *Neuroimage* **243** 118530

[81] Foo T K F *et al* 2020 Highly efficient head-only magnetic field insert gradient coil for achieving simultaneous high gradient amplitude and slew rate at 3.0T (MAGNUS) for brain microstructure imaging *Magn. Reson. Med.* **83** 2356–69

[82] Davids M, Dietz P, Ruyters G, Roesler M, Klein V, Guérin B, Feinberg D A and Wald L L 2023 Peripheral nerve stimulation informed design of a high-performance asymmetric head gradient coil *Magn. Reson. Med.* **90** 784–801

[83] Winkler S A, Schmitt F, Landes H, de Bever J, Wade T, Alejski A and Rutt B K 2018 Gradient and shim technologies for ultra high field MRI *Neuroimage* **168** 59–70
[84] Wu A *et al* 2024 Design and construction of a low-cryogen, lightweight, head-only 7T MRI magnet *IEEE Trans. Appl. Supercond.* **34** 1–5
[85] Stafford R J 2005 TU-B-I-617-01: high field MRI—technology, applications, safety, and limitations *Med. Phys.* **32** 2077
[86] Schaap K, Christopher-De Vries Y, Crozier S, De Vocht F and Kromhout H 2014 Exposure to static and time-varying magnetic fields from working in the static magnetic stray fields of MRI scanners: a comprehensive survey in the Netherlands *Ann. Occup. Hyg.* **58** 1094–110
[87] Batistatou E, Mölter A, Kromhout H, van Tongeren M V, Crozier S, Schaap K, Gowland P, Keevil S and de Vocht F 2015 Personal exposure to static and time-varying magnetic fields during MRI procedures in clinical practice in the UK *Occup. Environ. Med.* **73** 779–86
[88] Schenck J F 2013 Safety and sensory aspects of main and gradient fields in MRI *eMagRes* **2** 55–66
[89] Vijayalaxmi F M and Speck O 2015 Magnetic resonance imaging (MRI): a review of genetic damage investigations *Mutat. Res.* **764** 51–63
[90] Pophof B and Brix G 2024 Magnetic resonance imaging: recent research on the biological impacts of static magnetic and high-frequency electromagnetic fields *Imaging Radiat. Res.* **5** 66–72
[91] Grant A *et al* 2020 10.5 T MRI static field effects on human cognitive, vestibular, and physiological function *Magn. Reson. Imaging* **73** 163–76
[92] Rauschenberg J *et al* 2014 Multicenter study of subjective acceptance during magnetic resonance imaging at 7 and 9.4 T *Invest. Radiol.* **49** 249
[93] Antunes A, Glover P M, Li Y, Mian O S and Day B L 2012 Magnetic field effects on the vestibular system: calculation of the pressure on the cupula due to ionic current-induced Lorentz force *Phys. Med. Biol.* **57** 4477–87
[94] Mian O S, Li Y, Antunes A, Glover P M and Day B L 2013 On the vertigo due to static magnetic fields *PLoS* **8** e78748
[95] Thormann M, Amthauer H, Adolf D, Wollrab A, Ricke J and Speck O 2013 Efficacy of diphenhydramine in the prevention of vertigo and nausea at 7 T MRI *Eur. J. Radiol.* **82** 768–72
[96] Mian O S, Li Y, Antunes A, Glover P M and Day B L 2016 Effect of head pitch and roll orientations on magnetically induced vertigo *J. Physiol.* **594** 1051–67
[97] Houpt T A, Pittman D W, Riccardi C, Cassell J A, Lockwood D R, Barranco J M, Kwon B and Smith J C 2005 Behavioral effects on rats of high strength magnetic fields generated by a resistive electromagnet *Physiol. Behav.* **86** 379–89
[98] Houpt T A and Houpt C E 2010 Circular swimming in mice after exposure to a high magnetic field *Physiol. Behav.* **100** 284–90
[99] Wang S, Zheng M, Lou C, Chen S, Guo H, Gao Y, Lv H, Yuan X, Zhang X and Shang P 2022 Evaluating the biological safety on mice at 16 T static magnetic field with 700 MHz radio-frequency electromagnetic field *Ecotoxicol. Environ. Saf.* **230** 113125
[100] Khan M H, Huang X, Tian X, Ouyang C, Wang D, Feng S, Chen J, Xue T, Bao J and Zhang X 2022 Short- and long-term effects of 3.5–23.0 Tesla ultra-high magnetic fields on mice behaviour *Eur. Radiol.* **32** 5596–605
[101] Tkáč I, Benneyworth M A, Nichols-Meade T, Steuer E L, Larson S N, Metzger G J and Uğurbil K 2021 Long-term behavioral effects observed in mice chronically exposed to static ultra-high magnetic fields *Magn. Reson. Med.* **86** 1544–59
[102] Le Ster C, Selingue E, Poirier R, Edeline J-M, Mériaux S and Boulant N 2023 Behavioral and functional assessment of mice inner ear after chronic exposure to an ultrahigh B0 field of 11.7 T or 17.2 T *Magn. Reson. Med.* **90** 699–707
[103] Schenck J F 1996 The role of magnetic susceptibility in magnetic resonance imaging: MRI magnetic compatibility of the first and second kinds *Med. Phys.* **23** 815–50